Continuous monitoring of the dynamical Casimir effect with a damped detector

A. S. M. de Castro*
Universidade Estadual de Ponta Grossa, Departamento de Física, 84030-900 Ponta Grossa-PR, Brazil

V. V. Dodonov†
Universidade de Brasília, Instituto de Física, Caixa Postal 04455, 70910-900 Brasília-DF, Brazil

(Received 22 April 2014; published 18 June 2014)

We consider the problem of photon creation from vacuum inside an ideal cavity with harmonically vibrating walls in the resonance case, taking into account the interaction between the resonant field mode and a detector, modeled by a quantum damped harmonic oscillator. The frequency of wall vibrations is chosen to be exactly twice the cavity normal frequency. The field and detector modes are supposed to be initially in thermal quantum states with different temperatures. We analyze different regimes of excitation, characterized by the competition of three parameters: the modulation depth of the time-dependent cavity eigenfrequency, the cavity-detector coupling strength, and the detector damping coefficient. We show that statistical properties of the detector quantum state (variances of the photon numbers, photon distribution function, and the degree of quadrature squeezing) can be quite different from that of the field mode. In addition, the mean number of quanta in the detector mode increases with some time delay, compared with the field mode.

DOI: 10.1103/PhysRevA.89.063816 PACS number(s): 42.50.Pq, 42.50.Lc, 42.50.Ar

I. INTRODUCTION

The so-called dynamical Casimir effect (DCE), i.e., the creation of quanta from the initial vacuum (or thermal) state due to the motion of some boundaries or, more generally, fast variations of boundary conditions in cavities or quantum circuits, was the subject of numerous studies for the past decades (see Refs. [1–3] for recent reviews). However, the problem of detecting the Casimir photons and the back action of detectors on the rate of photon generation received much less attention until recently (although the first attempts were performed as far back as in Ref. [4]).

Different schemes based on atomic detectors were considered, e.g., in Refs. [5–8], but none of them were realized until now. On the other hand, in the real experiment under way in Padova/Legnaro (named MIR), the amplified electromagnetic field in superconducting niobium microwave cavities (whose fundamental resonance frequencies lie in the interval 1.5–2.5 GHz) is detected by means of a small induction loop, situated inside the cavity [9–11]. Since this loop is a part of an LC contour, it seems reasonable to model this kind of detector by a harmonic oscillator, coupled to the resonance field mode in the cavity. Such a model was analyzed recently in Refs. [12–14], where effects of dissipation were not taken into account. Indeed, the dissipation in the cavity walls can be neglected at the initial (exponential) stage of the amplification process, as soon as a sufficient amplification level is expected to be achieved after about 10^4 periods of the fundamental field mode oscillations in the cavity with quality factor exceeding the value of 10^6 [10]. (Of course, even small dissipation will become important for large times, and the final saturation level was a subject of some research [15,16], but at the current stage the experiments are performed in the exponential/unsaturated regime [11,17].)

Dissipation in the detector mode can be important because the induction loop is not in the superconducting state, so that the quality factor of the detector mode is much smaller than that of the cavity. Our aim is to analyze the influence of damping in the detecting tract on the rate of energy increase in the cavity and detector modes, as well as statistical properties of quantum states in both modes.

The model studied in the paper could seem very simple at first glance—two coupled harmonic oscillators. But, as a matter of fact, its analysis is not so simple, because one has to take into account many parameters. The resonance excitation of the selected field mode is described by minimum two parameters, even in the case of harmonic modulation of the cavity eigenfrequency (harmonic motion of boundary): the frequency of modulation and modulation depth. Coupling the mode (the first oscillator) to the detector (the second oscillator), one has to choose, in addition to a possible detuning between the frequencies of two modes, the form of coupling, together with the related coupling coefficients. In the most general case of bilinear coupling, one needs four coefficients, corresponding to possible terms $\hat{x}_1\hat{x}_2$, $\hat{p}_1\hat{p}_2$, $\hat{x}_1\hat{p}_2$, and $\hat{x}_2\hat{p}_1$, where $\hat{x}_j$ and $\hat{p}_j$ are generalized coordinates and momenta of the two oscillators ($j = 1,2$). In the case of time-independent frequencies, such a general coupling was considered, e.g., in Ref. [18].

In Refs. [12,14] we chose the coupling in the form $\hat{x}_1\hat{p}_2$ [4], in view of the standard minimal coupling term $-(e/c)\mathbf{pA}$, assuming that operator $\hat{x}_1$ is proportional to the vector potential of the field mode. It was shown that in many cases the detector responds to the change of the field state with a significant delay. Therefore it was supposed that effects of dissipation can be important. However, calculations turned out rather difficult for the coupling in that form, so that only approximate analytical solutions were obtained with the aid of the multiple scales method. On the other hand, calculations are much simpler if the coupling is taken in the form corresponding to the so-called rotating wave approximation (RWA) [13,19–21]. For this reason, we consider here the case of RWA coupling. It

*asmcastro@uepg.br
†vdodonov@fis.unb.br

is remarkable that such a choice permits us to obtain explicit analytical solutions (whose realm of validity is discussed in the concluding section).

The paper is organized as follows. In Sec. II we present the main dynamical equations and their analytical solutions in a general case. The concrete form of solutions for the specific choice of parameters used in this paper is given in Sec. III. These solutions are used in Sec. IV to obtain the time-dependent mean energies of each mode for the initial thermal equilibrium states, in two different regimes. In Secs. V–VII we calculate, respectively, the degree of squeezing in each mode, photon distribution functions, and the variances of the photon number operator. In Sec. VIII we discuss the results.

II. MAIN DYNAMICAL EQUATIONS

The simplest model describing the dynamical Casimir effect in an ideal cavity takes into account a single resonant cavity mode whose frequency is rapidly modulated according to the harmonical law $\omega_t = \omega_0[1 + \varepsilon \sin(\eta t)]$ with a small modulation depth, $|\varepsilon| \ll 1$. We shall use dimensionless variables, setting $\hbar = \omega_0 = 1$. Then the Hamiltonian for the resonance mode has the form [22]

$$\hat{H}_c = \omega_t \hat{n} - i\chi_t(\hat{a}^2 - \hat{a}^{\dagger 2}), \quad \chi_t = (4\omega_t)^{-1} d\omega_t/dt, \qquad (1)$$

where $\hat{a}$ and $\hat{a}^\dagger$ are the cavity annihilation and creation operators, and $\hat{n} \equiv \hat{a}^\dagger\hat{a}$ is the photon number operator. It is well known that the number of photons created from the initial vacuum state is maximal if the modulation frequency is exactly twice the unperturbed mode frequency, i.e., $\eta = 2$. The mean number of photons $\langle\hat{n}\rangle$ and the Mandel factor $Q = [\langle(\Delta\hat{n})^2\rangle - \langle\hat{n}\rangle]/\langle\hat{n}\rangle$ increase with time in this ideal case as (hereafter we use the subscript 0 for the quantities related to the empty cavity)

$$\langle\hat{n}_0(t)\rangle = \sinh^2(\varepsilon t/2), \quad Q_0(t) = 1 + 2\langle\hat{n}_0(t)\rangle. \qquad (2)$$

However, simple equations (2) hold for the ideal empty cavity only. To detect the emerging photons one has to couple the field mode to some detector. Here we consider the model of the detector as another harmonic oscillator, tuned to the same frequency as the selected field mode (obviously, any detuning between the two frequencies will diminish the detector efficiency). Choosing the RWA coupling between the oscillators, we arrive at the time-dependent Hamiltonian

$$\hat{H} = \omega_t\hat{a}_1^\dagger\hat{a}_1 + \hat{a}_2^\dagger\hat{a}_2 + g(\hat{a}_1\hat{a}_2^\dagger + \hat{a}_2\hat{a}_1^\dagger) - i\chi_t\big(\hat{a}_1^2 - \hat{a}_1^{\dagger 2}\big), \qquad (3)$$

where the coupling constant g is assumed to be real. Performing the time-dependent canonical transformation $\psi_t = \hat{U}_t\psi_t'$ with $\hat{U}_t = \exp[-it(\hat{a}_1^\dagger\hat{a}_1 + \hat{a}_2^\dagger\hat{a}_2)]$, we transform the initial Schrödinger equation $i\partial\psi/\partial t = \hat{H}\psi$ into $i\partial\psi'/\partial t = \hat{H}'\psi'$ with the new Hamiltonian $\hat{H}' = \hat{U}^\dagger\hat{H}\hat{U} - i\hat{U}^\dagger\partial\hat{U}/\partial t$, which does not contain the terms $\hat{a}_1^\dagger\hat{a}_1 + \hat{a}_2^\dagger\hat{a}_2$. The next step is to use again the rotating wave approximation, deleting all rapidly oscillating terms [containing factors $\exp(\pm ikt)$ with integral nonzero values of k] from Hamiltonian $\hat{H}'$. In addition, since the frequency modulation depth ε is small under realistic laboratory conditions (as well as coupling constant g), we maintain only linear terms with respect to this parameter, neglecting terms proportional to ε^2. Assuming that the modulation frequency equals $\eta = 2$, we obtain the time-independent Hamiltonian

$$\hat{H}'' = g(\hat{a}_1\hat{a}_2^\dagger + \hat{a}_2\hat{a}_1^\dagger) - i\beta\big(\hat{a}_1^2 - \hat{a}_1^{\dagger 2}\big), \quad \beta \equiv \varepsilon/4. \qquad (4)$$

To take into account damping in the detector mode, we follow the usual scheme, replacing the Schrödinger equation $i\partial\psi'/\partial t = \hat{H}''\psi'$ by the standard master equation for the statistical operator $\hat{\rho}$:

$$\frac{d\hat{\rho}}{dt} = -i[\hat{H}'',\hat{\rho}] - \gamma\nu(\hat{a}_2\hat{a}_2^\dagger\hat{\rho} + \hat{\rho}\hat{a}_2\hat{a}_2^\dagger - 2\hat{a}_2^\dagger\hat{\rho}\hat{a}_2) - \gamma(1+\nu)(\hat{a}_2^\dagger\hat{a}_2\hat{\rho} + \hat{\rho}\hat{a}_2^\dagger\hat{a}_2 - 2\hat{a}_2\hat{\rho}\hat{a}_2^\dagger), \qquad (5)$$

where $\gamma > 0$ is the damping coefficient, and $\nu \geqslant 0$ is the mean number of excitations in a thermal reservoir coupled to the detector.

It is convenient to introduce the four-dimensional vector $\hat{\mathbf{y}} = (\hat{a}_1, \hat{a}_1^\dagger, \hat{a}_2, \hat{a}_2^\dagger)$. Its mean value $\langle\hat{\mathbf{y}}\rangle \equiv \mathrm{Tr}(\hat{\rho}\hat{\mathbf{y}})$ obeys the equation

$$d\langle\hat{\mathbf{y}}\rangle/dt = \mathbf{A}\langle\hat{\mathbf{y}}\rangle, \qquad (6)$$

where the 4×4 evolution matrix $\mathbf{A}$ has the form

$$\mathbf{A} = \begin{bmatrix} 0 & 2\beta & -ig & 0 \\ 2\beta & 0 & 0 & ig \\ -ig & 0 & -\gamma & 0 \\ 0 & ig & 0 & -\gamma \end{bmatrix} \equiv \begin{bmatrix} 2\beta\sigma_x & -ig\sigma_z \\ -ig\sigma_z & -\gamma\sigma_0 \end{bmatrix}. \qquad (7)$$

Here σ_x and σ_z are the standard 2×2 Pauli matrices, whereas σ_0 means the 2×2 unity matrix. The 4×4 *symmetrical* covariance matrix $\mathbf{M}$ with elements $M_{jk} = \mathrm{Tr}[\hat{\rho}(\hat{y}_j\hat{y}_k + \hat{y}_k\hat{y}_j)]/2 - \langle\hat{y}_j\rangle\langle\hat{y}_k\rangle$ obeys the equation

$$d\mathbf{M}/dt = \mathbf{A}\mathbf{M} + \mathbf{M}\tilde{\mathbf{A}} + \mathbf{D}, \qquad (8)$$

where the tilde above $\mathbf{A}$ means the transposed matrix. The diffusion matrix $\mathbf{D}$ has one nonzero 2×2 block only:

$$\mathbf{D} = \begin{bmatrix} \mathbf{0} & \mathbf{0} \\ \mathbf{0} & \mathbf{D}_2 \end{bmatrix}, \quad \mathbf{D}_2 = 2\gamma\tilde{\nu}\sigma_x, \quad \tilde{\nu} = \nu + 1/2. \qquad (9)$$

The solutions to Eqs. (6) and (8) are given by equations

$$\langle\hat{\mathbf{y}}\rangle_t = \mathbf{U}(t)\langle\hat{\mathbf{y}}\rangle_0, \qquad (10)$$

$$\mathbf{M}_t = \mathbf{U}(t)\mathbf{M}_0\tilde{\mathbf{U}}(t) + \int_0^t d\tau\mathbf{U}(t-\tau)\mathbf{D}\tilde{\mathbf{U}}(t-\tau), \qquad (11)$$

where

$$\mathbf{U}(t) = \exp(\mathbf{A}t). \qquad (12)$$

It is convenient to use the block forms for matrices $\mathbf{M}$ and $\mathbf{U}$, as well,

$$\mathbf{M} = \begin{bmatrix} \mathbf{M}_1 & \mathbf{M}_{12} \\ \mathbf{M}_{21} & \mathbf{M}_2 \end{bmatrix}, \quad \mathbf{U} = \begin{bmatrix} \mathbf{U}_1 & \mathbf{U}_{12} \\ \mathbf{U}_{21} & \mathbf{U}_2 \end{bmatrix}. \qquad (13)$$

Matrix $\mathbf{M}$ is symmetric, $\tilde{\mathbf{M}} = \mathbf{M}$, due to its definition. But the evolution matrix $\mathbf{U}(t)$ is symmetric as well, due to the specific property $\tilde{\mathbf{A}} = \mathbf{A}$ of matrix (7). We assume that initially the field mode and the detector were uncorrelated, i.e.,

$\mathbf{M}_{12}(0) = \mathbf{M}_{21}(0) = \mathbf{0}$. Then the 2×2 blocks of matrix $\mathbf{M}(t)$ can be written as follows,

$$\mathbf{M}_1(t) = \mathbf{U}_1\mathbf{M}_1(0)\mathbf{U}_1 + \mathbf{U}_{12}\mathbf{M}_2(0)\mathbf{U}_{21} + \int_0^t \mathbf{U}_{12}(t-\tau)\mathbf{D}_2\mathbf{U}_{21}(t-\tau)d\tau, \quad (14)$$

$$\mathbf{M}_2(t) = \mathbf{U}_2\mathbf{M}_2(0)\mathbf{U}_2 + \mathbf{U}_{21}\mathbf{M}_1(0)\mathbf{U}_{12} + \int_0^t \mathbf{U}_2(t-\tau)\mathbf{D}_2\mathbf{U}_2(t-\tau)d\tau, \quad (15)$$

$$\mathbf{M}_{12}(t) = \mathbf{U}_1\mathbf{M}_1(0)\mathbf{U}_{12} + \mathbf{U}_{12}\mathbf{M}_2(0)\mathbf{U}_2 + \int_0^t \mathbf{U}_{12}(t-\tau)\mathbf{D}_2\mathbf{U}_2(t-\tau)d\tau. \quad (16)$$

III. EVOLUTION MATRIX AND CONDITIONS FOR THE PHOTON GENERATION

The evolution matrix $\mathbf{U}(t)$ can be easily found, if one knows the roots of the characteristic equation $p(z)\equiv \det(\mathbf{A}-z\mathbf{E})=0$ (where $\mathbf{E}$ is the 4×4 unity matrix). This is the complete fourth-order algebraic equation

$$z^4 + h_1 z^3 + h_2 z^2 + h_3 z + h_4 = 0, \quad (17)$$

with the following coefficients:

$$h_2 = 2(g^2 - 2\beta^2) + \gamma^2, \quad h_4 = g^4 - 4\gamma^2\beta^2, \quad (18)$$

$$h_1 = 2\gamma, \quad h_3 = 2\gamma(g^2 - 4\beta^2). \quad (19)$$

Fortunately, Eq. (17) with coefficients given by Eqs. (18) and (19) can be solved analytically (actually, this was done with the aid of the MAPLE program). Four roots can be written as $\beta_- \pm R_+$ and $\beta_+ \pm R_-$, where

$$\beta_\pm = \pm\beta - (\gamma/2), \quad R_\pm = \sqrt{\beta_\pm^2 - g^2}. \quad (20)$$

Then the standard procedure leads to the following explicit equations for the elements of evolution matrix in terms of the Pauli matrices:

$$\mathbf{U}_1 = \frac{1}{2}(F_+\sigma_0 + F_-\sigma_x), \quad (21)$$

$$\mathbf{U}_2 = \frac{1}{2}(K_+\sigma_0 - K_-\sigma_x), \quad (22)$$

$$\mathbf{U}_{12} = -\frac{g}{2}(iG_+\sigma_z + G_-\sigma_y), \quad (23)$$

where

$$F_\pm = E_+(C_- - \beta_- S_-) \pm E_-(C_+ - \beta_+ S_+), \quad (24)$$

$$K_\pm = E_+(C_- + \beta_- S_-) \pm E_-(C_+ + \beta_+ S_+), \quad (25)$$

$$G_\pm = E_+ S_- \pm E_- S_+, \quad (26)$$

$$E_\pm = e^{\beta_\pm t}, \quad C_\pm = \cosh(R_\pm t), \quad S_\pm = \frac{\sinh(R_\pm t)}{R_\pm}.$$

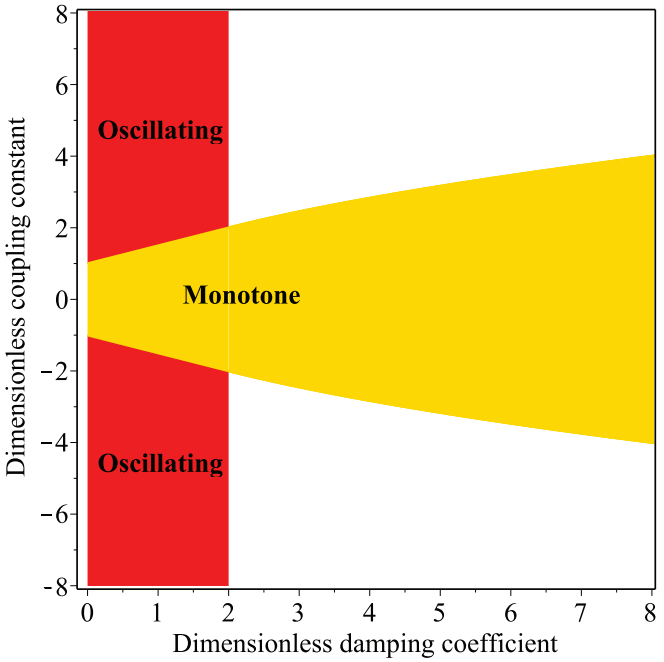

FIG. 1. (Color online) The regions in the parameter plane $\gamma/(\beta\omega_0)$-$g/(\beta\omega_0)$, where photon generation from vacuum is possible. The yellow horizontal region corresponds to the monotone regime of photon generation (real values of coefficient R_-): see Sec. IV A. The red vertical domain corresponds to imaginary values of R_-. Here the exponential growth of the mean photon numbers is modulated by oscillations, discussed in Sec. IV B.

Obviously, the real parts of the roots $\beta_- \pm R_+$ never can be positive for non-negative values of parameters β and γ. On the other hand, the real part of the root $\beta_+ + R_-$ is positive for $\gamma < 2\beta$ and any value of the real coupling constant g. Moreover, if $\gamma > 2\beta$ (i.e., $\beta_+ < 0$), nonetheless the sum $\beta_+ + R_-$ can be positive, provided $2\gamma\beta > g^2$. This can be easily seen from the equation

$$R_- - |\beta_+| = \frac{2\beta\gamma - g^2}{R_- + |\beta_+|}.$$

The regions of photon generation in the $\gamma - g$ parameter plane are shown in Fig. 1. They are confined by the vertical line $\gamma = 0, -\infty < g < \infty$, two vertical lines $\gamma = 2\beta, |g| \geqslant 2\beta$, and two pieces of parabolas $g = \pm\sqrt{2\gamma\beta}, \gamma \geqslant 2\beta$. The yellow part of this region (in the online version of the paper), confined between the straight line segments $|g| = \beta + \gamma/2$ for $\gamma \leqslant 2\beta$ and the parabolas $|g| = \sqrt{2\gamma\beta}$ for $\gamma \geqslant 2\beta$, corresponds to real values of coefficient R_-. In this domain, the monotone regime of photon generation is observed: see Sec. IV A. The red domain, confined by the vertical lines $\gamma = 0$, $\gamma = 2\beta$, and the straight line segments $|g| = \beta + \gamma/2$, corresponds to imaginary values of R_-. Here the exponential growth of the mean photon numbers is modulated by oscillations, discussed in Sec. IV B.

In order to avoid confusion, it is worth emphasizing that all figures are made for dimensionless variables. Parameter $\beta = \varepsilon/4$ is the dimensionless frequency modulation depth, which is very small under realistic conditions. For real oscillating boundaries, it hardly can exceed the value 10^{-8} [4]. In

attempts to simulate the motion of boundaries, using periodic laser excitations of thin semiconductor slabs [9] or nonlinear optical crystals/fibers [23,24], one may hope to achieve the level of $\beta \sim 10^{-3}$. The coupling constant g and damping coefficient γ have the dimensionality of frequency, but they are normalized by the cavity fundamental eigenfrequency ω_0. Therefore the values of dimensionless coupling constant and dimensionless damping coefficient in the vertical and horizontal axes in Fig. 1 (and other figures) mean the ratios $g/(\beta\omega_0)$ and $\gamma/(\beta\omega_0) = (2Q_d\beta)^{-1}$, respectively (where Q_d is the quality factor of the detector mode).

IV. COVARIANCE MATRIX AND MEAN ENERGIES

We suppose that each mode ($k = 1,2$) was initially in a thermal state with the dimensionless mean energy $\vartheta_k \geqslant 1/2$ (actually $\hbar\omega_0\vartheta_k$), i.e., $\mathbf{M}_k(0) = \vartheta_k\sigma_x$. Then Eqs. (14)–(16) and (21)–(23) lead to the equations

$$\mathbf{M}_k(t) = \mathcal{E}_k(t)\sigma_x + \mathcal{B}_k(t)\sigma_0. \tag{27}$$

Obviously, $\mathcal{E}_k(t)$ is nothing but the time-dependent mean energy of the kth mode (normalized by $\hbar\omega_0$), whereas $\mathcal{B}_k(t)$ is the time-dependent mean value of dimensionless operator $\hat{a}_k^2$. The characteristic temperature $T_0 = \hbar\omega_0/k_B \sim 0.1$ K for $\omega_0/(2\pi) \sim 2$ GHz. Therefore parameters ϑ_k are big for low-frequency microwave cavities, even for helium temperatures. Nonetheless, there are no physical limitations for smaller values of ϑ_k. One can achieve the values $\vartheta_k \sim 1$, using cavities with higher resonance frequencies and lowering temperatures down to the sub-Kelvin region. Therefore, comparing the temperature effects with the ideal results (obtained for the initial vacuum states of the cavity and detector modes), we use not very big values of ϑ_k for illustrations in this and subsequent sections, in order to make figures more compact.

Explicit expressions for the functions $\mathcal{E}_k(t)$ and $\mathcal{B}_k(t)$ are as follows,

$$\mathcal{E}_1(t) = \frac{1}{4}[\vartheta_1(F_+^2 + F_-^2) + g^2\vartheta_2(G_+^2 + G_-^2)]_t + \frac{\gamma}{2}\tilde{\nu}g^2\int_0^t d\tau(G_+^2 + G_-^2)_\tau, \tag{28}$$

$$\mathcal{E}_2(t) = \frac{1}{4}[\vartheta_2(K_+^2 + K_-^2) + g^2\vartheta_1(G_+^2 + G_-^2)]_t + \frac{\gamma}{2}\tilde{\nu}\int_0^t d\tau(K_+^2 + K_-^2)_\tau, \tag{29}$$

$$\mathcal{B}_1(t) = \frac{1}{2}[\vartheta_1 F_+F_- + g^2\vartheta_2 G_+G_-]_t + \gamma\tilde{\nu}g^2\int_0^t d\tau(G_+G_-)_\tau, \tag{30}$$

$$\mathcal{B}_2(t) = -\frac{1}{2}[\vartheta_2 K_+K_- + g^2\vartheta_1 G_+G_-]_t - \gamma\tilde{\nu}\int_0^t d\tau\,(K_+K_-)_\tau\,, \tag{31}$$

where the subscripts t or τ stand for the arguments of time-dependent functions $F_\pm$, $G_\pm$, and $K_\pm$. Performing the integrations over $d\tau$ we get

$$\mathcal{E}_1(t) = \frac{1}{4}[\vartheta_1(F_+^2 + F_-^2) + g^2\vartheta_2(G_+^2 + G_-^2)]_t + \frac{\gamma}{2}\tilde{\nu}g^2(\Phi_+ + \Phi_-), \tag{32}$$

$$\mathcal{B}_1(t) = \frac{1}{2}[\vartheta_1 F_+F_- + g^2\vartheta_2 G_+G_-]_t + \frac{\gamma}{2}\tilde{\nu}g^2(\Phi_+ - \Phi_-), \tag{33}$$

$$\mathcal{E}_2(t) = \frac{1}{4}[\vartheta_2(K_+^2 + K_-^2) + g^2\vartheta_1(G_+^2 + G_-^2)]_t + \frac{\gamma}{2}\tilde{\nu}(\Psi_+ + \Psi_-), \tag{34}$$

$$\mathcal{B}_2(t) = -\frac{1}{2}[\vartheta_2 K_+K_- + g^2\vartheta_1 G_+G_-]_t - \frac{\gamma}{2}\tilde{\nu}(\Psi_+ - \Psi_-), \tag{35}$$

where

$$\Phi_\pm = \frac{E_\pm}{\Gamma_\mp}[E_\pm S_\mp(\beta_\pm S_\mp - C_\mp) + \tilde{S}_\pm], \tag{36}$$

$$\Psi_\pm = \frac{E_\pm}{\Gamma_\mp}\{E_\pm S_\mp[\eta_\pm S_\mp + C_\mp(g^2 \pm 4\beta\beta_\mp)] + \tilde{S}_\pm(g^2 \pm 4\beta\beta_\pm)\}, \tag{37}$$

$$\Gamma_\pm = g^2 \pm 2\beta\gamma, \quad \tilde{S}_\pm = \sinh(\beta_\pm t)/\beta_\pm, \tag{38}$$

$$\eta_\pm = g^2(\mp 3\beta - \gamma/2) \pm 4\beta\beta_\mp^2. \tag{39}$$

In all illustrations below we assume that $\tilde{\nu} = \vartheta_2$. Then $\mathcal{E}_2 = $ const. in the absence of coupling, $g = 0$, so that changes of $\mathcal{E}_2$ are due to the interaction with the field mode only. The most interesting quantities are asymptotic values of mean energies in the long time limit. It is easy to see that only terms containing functions G_+, K_+, F_+, Φ_+ and Ψ_+ can give an exponential increase of mean energies in Eqs. (32) and (34), whereas terms containing counterparts of these functions with the subscript "−" can be neglected in this limit, since they either decay with time or remain constant. There are two asymptotic regimes of excitations.

A. Asymptotic monotone regime

Coefficient R_- is real if $|g| < \beta + \gamma/2$ (we assume that $\beta,\gamma \geqslant 0$). In this case we have in the long time limit

$$\mathcal{E}_1(t) \approx \frac{1}{8R_-^2}\exp[2(\beta_+ + R_-)t] \times\left[\vartheta_1(R_- - \beta_-)^2 + g^2\left(\vartheta_2 + \frac{\gamma\tilde{\nu}}{\beta_+ + R_-}\right)\right], \tag{40}$$

$$\mathcal{E}_2(t) \approx \frac{1}{8R_-^2}\exp[2(\beta_+ + R_-)t]\left\{\vartheta_2(R_- + \beta_-)^2 + g^2\vartheta_1 + \frac{\gamma\tilde{\nu}}{\Gamma_-}[\eta_+ + R_-(g^2 + 4\beta\beta_-)]\right\}. \tag{41}$$

Typical plots of functions $\ln[2\mathcal{E}_{1,2}(t)]$ in the monotone regime are shown in Fig. 2 for different values of parameters (remember that dimensionless time means in fact the product

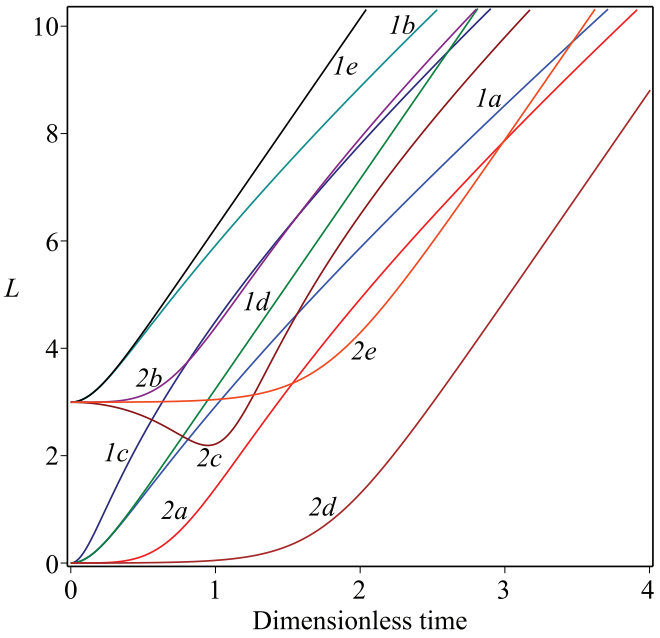

FIG. 2. (Color online) Dimensionless functions $L \equiv \ln[2\mathcal{E}_{1,2}]$ versus the dimensionless time variable $\beta\omega_0 t$ in the monotone regime with $\beta = g/\omega_0$ and $\tilde{\nu} = \vartheta_2$, for the cavity (*1*) and detector (*2*) modes. The labels (a,b,c) correspond to the case of $\gamma = 0$, whereas $\gamma = 20\beta\omega_0$ in the cases (d,e). Also, (a,d) and (b,e) correspond respectively to the vacuum ($\vartheta_1 = \vartheta_2 = 0.5$) and thermal ($\vartheta_1 = \vartheta_2 = 10$) initial states in both modes. In case of (c) the cavity is initially in the vacuum ($\vartheta_1 = 0.5$) and detector in the thermal state ($\vartheta_2 = 10$).

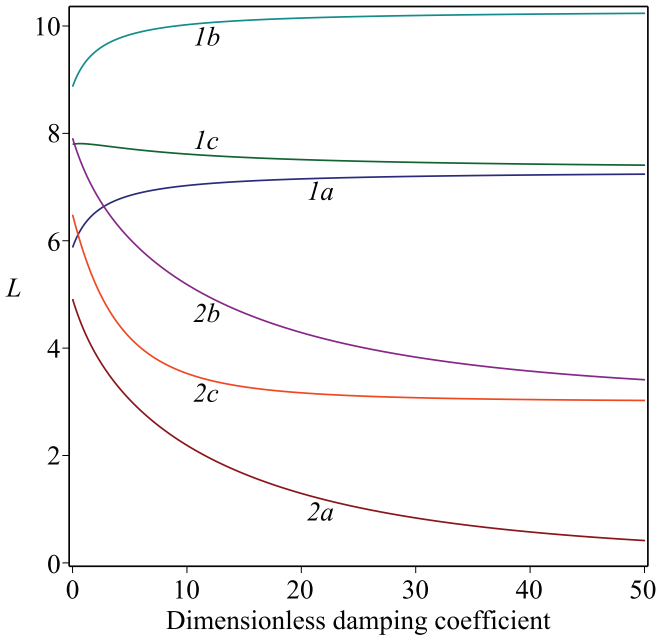

FIG. 3. (Color online) Dimensionless functions $L \equiv \ln[2\mathcal{E}_{1,2}]$ versus the dimensionless damping coefficient $\gamma/(\beta\omega_0)$ in the monotone regime, for $t = 2/(\beta\omega_0)$, $\beta = g/\omega_0$, and $\tilde{\nu} = \vartheta_2$. Labels *1* and *2* correspond to the cavity and detector modes, respectively. In case (a) both modes are initially in the vacuum states ($\vartheta_1 = \vartheta_2 = 1/2$). In case (b) both modes are initially in the identical thermal states with $\vartheta_1 = \vartheta_2 = 10$. In case (c) the cavity starts in the vacuum ($\vartheta_1 = 0.5$) and detector in the thermal state with $\vartheta_2 = 10$.

$\beta\omega_0 t$). We see that the response of the detector diminishes (the delay time increases) with increasing damping coefficient. Such a behavior seems quite expected. What is unexpected is the behavior of the mean energy in the cavity mode: this quantity *increases* with increasing damping in the detector mode (for fixed other parameters). This can be explained, partially, by the behavior of the quantity $\beta_+ + R_- = \beta - \gamma/2 + \sqrt{(\beta+\gamma/2)^2 - g^2}$, which stands in the argument of exponential function in Eq. (40). This quantity grows monotonously as function of γ, from some minimal value ($\beta + \sqrt{\beta^2 - g^2}$ if $|g| < \beta$, or $2\beta - |g|$ if $|g| > \beta$) to 2β as $\gamma \to \infty$. But preexponential factors in Eqs. (40) and (41) are also important. Figure 3 shows the dependence of the mean energies of two modes on the damping coefficient, for different sets of other parameters and a fixed value of time. One can see that situations when $\mathcal{E}_1(t)$ decreases with γ are also possible, depending on the initial conditions. If $|g| \ll \beta + \gamma/2$ (including the case of very strong damping in the detector channel), then

$$\mathcal{E}_1(t) \approx \exp\left[\left(2\beta - \frac{g^2}{|\beta_-|}\right)t\right]\left[\frac{\vartheta_1}{2} + \frac{g^2}{8\beta_-^2}\left(\vartheta_2 + \frac{\gamma\tilde{\nu}}{2\beta}\right)\right], \tag{42}$$

$$\mathcal{E}_2(t) \approx \frac{g^2\vartheta_1}{8\beta_-^2}\exp\left[\left(2\beta - \frac{g^2}{|\beta_-|}\right)t\right]. \tag{43}$$

Neglected terms in Eq. (43) (which depend on the initial parameter ϑ_2 of the detector and the reservoir temperature parameter $\tilde{\nu}$) are either proportional to g^4, or they do not show the exponential growth with time. In this case, the detector is excited for any damping coefficient, but its response is suppressed by the factor $g^2/4\beta_-^2$ (or g^2/γ^2 if $\gamma \gg \beta$), compared with the mean energy of the field mode. This suppression can be also interpreted as the time delay $\delta t \approx \beta^{-1}\ln(2|\beta_-|/|g|)$ of the response of the detector. This effect of time delay was discovered in the special nondissipative case in Refs. [12,14]. On the other hand, even very strong damping does not influence the mean energy of the field mode, according to Eq. (42).

B. Asymptotic oscillating regime

If $|g| > \beta + \gamma/2$, then coefficient R_- is imaginary. In this case the asymptotical exponential growth of energies is modulated by oscillating functions $c_-(t) = \cos(|R_-|t)$ and $s_-(t) = \sin(|R_-|t)/|R_-|$:

$$\mathcal{E}_1(t) \approx \exp(2\beta_+ t)\left\{\frac{1}{4}[\vartheta_1(c_- - \beta_- s_-)^2 + g^2\vartheta_2 s_-^2] + \frac{\gamma\tilde{\nu}g^2}{2\Gamma_-}\left[s_-(\beta_+ s_- - c_-) + \frac{1}{2\beta_+}\right]\right\}, \tag{44}$$

$$\mathcal{E}_2(t) \approx \exp(2\beta_+ t)\left\{\frac{1}{4}[\vartheta_2(c_- + \beta_- s_-)^2 + g^2\vartheta_1 s_-^2] + \frac{\gamma\tilde{\nu}}{2\Gamma_-}\left[\eta_+ s_-^2 + s_- c_-(g^2 + 4\beta\beta_-) + \frac{g^2}{2\beta_+} + 2\beta\right]\right\}. \tag{45}$$

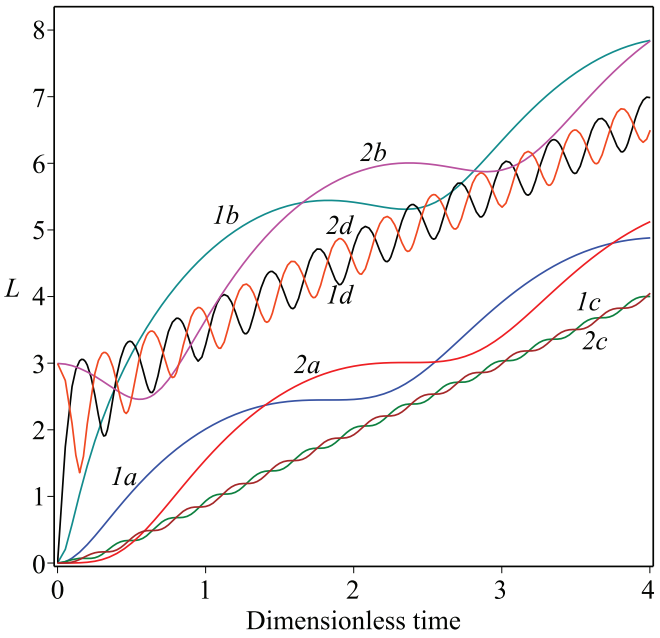

FIG. 4. (Color online) Dimensionless functions $L \equiv \ln[2\mathcal{E}_{1,2}]$ versus the dimensionless time variable $\beta\omega_0 t$ in the oscillating regime with $\beta = \gamma/\omega_0$ and $\tilde{\nu} = \vartheta_2$, for the cavity (*1*) and detector (*2*) modes. The cases (a,b) and (c,d) correspond to the values $g = 2\beta\omega_0$ and $g = 10\beta\omega_0$, respectively. The initial thermal parameters are $\vartheta_1 = \vartheta_2 = 0.5$ in the cases (a,c), and $\vartheta_1 = 0.5$, $\vartheta_2 = 10$ in the cases (b,d).

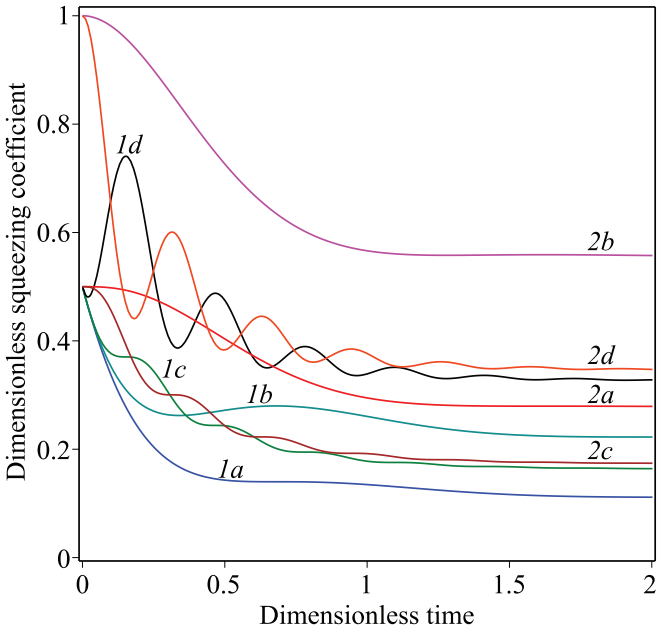

FIG. 5. (Color online) Dimensionless squeezing coefficient $\chi = \mathcal{E} - |\mathcal{B}|$ versus the dimensionless time variable $\beta\omega_0 t$ in the oscillating regime with $\beta = \gamma/\omega_0$ and $\tilde{\nu} = \vartheta_2$, for the cavity (*1*) and detector (*2*) modes. The cases (a,b) and (c,d) correspond to the values $g = 2\beta\omega_0$ and $g = 10\beta\omega_0$, respectively. The initial thermal parameters are $\vartheta_1 = \vartheta_2 = 0.5$ in the cases (a,c), and $\vartheta_1 = 0.5$, $\vartheta_2 = 1$ in the cases (b,d).

Typical plots of functions $\mathcal{E}_{1,2}(t)$ in the oscillating regime are shown in Fig. 4. For $|g| \gg \beta,\gamma$ we see a fast energy exchange between the two modes, with a relatively slow exponential increase of the total energy (a similar behavior of energies of two coupled modes in different DCE configurations was found in Refs. [12,14,25,26]). In this case $\Gamma_- \approx |R_-|^2 \approx g^2$. Therefore, neglecting terms of the order of $|\beta_-/g|$, we obtain simple equations

$$\mathcal{E}_1(t) \approx \tfrac{1}{4}e^{2\beta_+ t}[\vartheta_1\cos^2(gt) + \vartheta_2\sin^2(gt) + \gamma\tilde{\nu}/\beta_+], \quad (46)$$

$$\mathcal{E}_2(t) \approx \tfrac{1}{4}e^{2\beta_+ t}[\vartheta_2\cos^2(gt) + \vartheta_1\sin^2(gt) + \gamma\tilde{\nu}/\beta_+]. \quad (47)$$

V. SQUEEZING

The degree of squeezing in each mode is characterized by the minimal value of variance of any dimensionless quadrature component taken over the period of fast oscillations with the frequency $2\omega_0$ [26,27] (this is equivalent to the principal squeezing introduced in Ref. [28]). It is given by a simple equation

$$\chi_k = \mathcal{E}_k - |\mathcal{B}_k|. \quad (48)$$

The state is squeezed if $\chi_k < 1/2$. Equation (48) shows that values of coefficients χ_k depend on the signs of functions $\mathcal{B}_k$. It appears that function $\mathcal{B}_1(t)$ with $t > 0$ is positive for all possible sets of parameters. Then, using Eqs. (32) and (33), we can write (48) in the following explicit form:

$$\chi_1 = E_-^2[\vartheta_1(C_+ - \beta_+ S_+)^2 + \vartheta_2 g^2 S_+^2] + \gamma\tilde{\nu}g^2\Phi_-. \quad (49)$$

Function $\mathcal{B}_2(t)$ is negative for $t > 0$ and all other parameters under the condition $\vartheta_2 < 3\vartheta_1$. This inequality follows from the Taylor expansion in the short time limit, $\mathcal{B}_2(t) = 2t^3\beta g^2(\vartheta_2/3 - \vartheta_1) + \mathcal{O}(t^4)$. If $\vartheta_2 > 3\vartheta_1$, then initially $\mathcal{B}_2(t) > 0$, but this function changes sign at some moment t_*, which is of the order of β^{-1} for $\vartheta_2 \gg \vartheta_1$, becoming much smaller when $\vartheta_2 \to 3\vartheta_1$. The explicit expression of function $\chi_2(t)$ for $\mathcal{B}_2(t) < 0$ reads

$$\chi_2 = E_-^2[\vartheta_2(C_+ + \beta_+ S_+)^2 + \vartheta_1 g^2 S_+^2] + \gamma\tilde{\nu}\Psi_-. \quad (50)$$

This equation is valid for any value of time variable t if $\vartheta_2 < 3\vartheta_1$ and for $t > t_*$ if $\vartheta_2 > 3\vartheta_1$. Plots of functions $\chi_k(t)$ in the oscillating regime are shown in Fig. 5.

If $\gamma = 0$, then both squeezing coefficients, χ_1 and χ_2, go asymptotically to zero as $t \to \infty$, for any values of parameters g and ϑ_k, in agreement with Ref. [14]. But if $\gamma > 0$, then the product $E_-\tilde{S}_-$ in functions $\Phi_-(t)$ and $\Psi_-(t)$ tends to a finite limit as $t \to \infty$, whereas the terms containing ϑ_k in (49) and (50) go to zero. Therefore, both squeezing coefficients tend to the asymptotic finite values $\chi_k(\infty)$, which do not depend on the initial states:

$$\chi_1(\infty) = \frac{\gamma\tilde{\nu}g^2}{(g^2 + 2\beta\gamma)(2\beta + \gamma)}, \quad (51)$$

$$\chi_2(\infty) = \frac{\gamma\tilde{\nu}(g^2 + 2\beta\gamma + 4\beta^2)}{(g^2 + 2\beta\gamma)(2\beta + \gamma)}. \quad (52)$$

Equations (51) and (52) hold in all regimes, even in the cases when there is no asymptotic growth of the mean energies. Note that $\chi_1(\infty) < \chi_2(\infty)$, i.e., the field mode is asymptotically

more squeezed than the detector one. In addition, both coefficients $\chi_k(\infty)$ obey the inequality $\chi_k(\infty) < \tilde{\nu}$ $(k = 1,2)$. Consequently, for a zero-temperature reservoir $(\tilde{\nu} = 1/2)$, both modes become squeezed asymptotically for any values of g and γ. An interesting feature of $\chi_1(\infty)$ as function of the damping coefficient is the existence of maximum $\chi_1^{\max}(\infty) = \tilde{\nu} g^2/(2\beta + g)^2$ at $\gamma = |g|$. Moreover, $\chi_1(\infty)$ goes to zero for $\gamma \to \infty$. On the contrary, $\chi_2(\infty)$ is monotone function of γ, going to $\tilde{\nu}$ as $\gamma \to \infty$. For $\tilde{\nu} > 1/2$ (or $\nu > 0$), squeezing of the field mode can be achieved inside the following domain:

$$\begin{aligned} &\gamma < \beta/\nu: && \text{arbitrary } g \\ &\gamma > \beta/\nu: && g^2 < \frac{\beta\gamma(2\beta+\gamma)}{\gamma\nu - \beta}. \end{aligned} \tag{53}$$

On the other hand, $\chi_2(\infty) < 1/2$ if

$$\gamma < \beta/\nu \quad \text{and} \quad g^2 > \frac{2\nu\beta\gamma(2\beta+\gamma)}{\beta - \gamma\nu} \tag{54}$$

[for example, $\chi_2(\infty) = \tilde{\nu}$ if $g = 0$]. The intersection of both domains is illustrated in Fig. 6.

VI. PHOTON DISTRIBUTION FUNCTIONS

The photon distribution function (PDF) of the Gaussian states was derived in Refs. [29–31]. For zero mean values of quadrature components $\hat{x}$ and $\hat{p}$ it can be expressed in terms

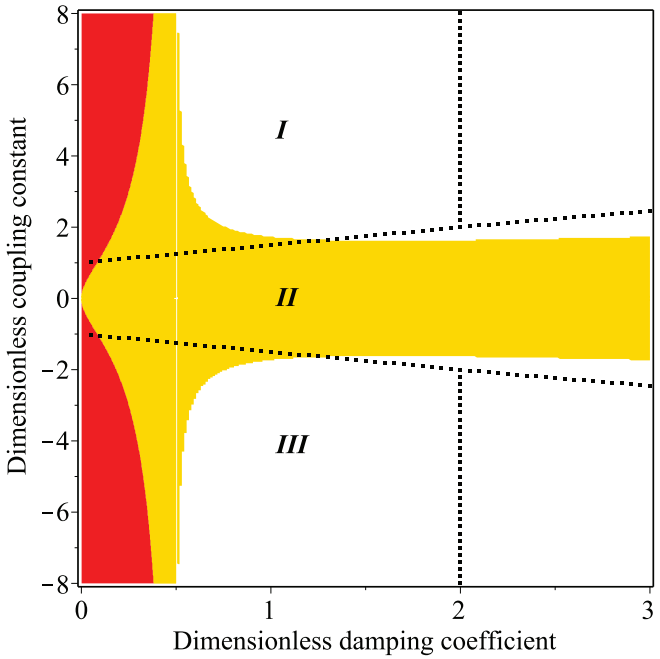

FIG. 6. (Color online) The red region to the right of the vertical axis corresponds to intersection of the domains (53) and (54) in the parameter plane $\gamma/(\beta\omega_0)$-$g/(\beta\omega_0)$, where both the field and detector modes can be squeezed asymptotically, for $\nu = 2$. In the yellow region, only the field mode can be squeezed. Regions *I* and *III*, delimited by point lines, correspond to the oscillating regime, while the region *II* refers to the monotone regime of photon generation.

of the Legendre polynomials $P_k(x)$ as [32]

$$\mathcal{P}(k) = \frac{Y_-^{k/2}}{Y_+^{(k+1)/2}} P_k\left(\frac{Y}{\sqrt{Y_+ Y_-}}\right), \tag{55}$$

where

$$Y = \mathcal{E}^2 - |\mathcal{B}|^2 - 1/4, \tag{56}$$

$$Y_\pm = (\mathcal{E} \pm 1/2)^2 - |\mathcal{B}|^2 = Y \pm \mathcal{E} + 1/2. \tag{57}$$

It can be shown that $Y \geqslant 0$ for any quantum state (this inequality is one of several equivalent forms of the Schrödinger-Robertson uncertainty relation [33]). Therefore $Y_+ > 0$, but the quantity Y_- can be positive or negative. The normalization condition $\sum_{k=0}^{\infty} k\mathcal{P}(k) = 1$ is fulfilled due to the known generating function of the Legendre polynomials

$$\sum_{k=0}^{\infty} z^k P_k(x) = [1 - 2xz + z^2]^{-1/2}.$$

The behavior of PDF as function of k depends on the value of the argument of the Legendre polynomial. If this argument is close to zero, then strong oscillations of function $\mathcal{P}(k)$ are observed, since Legendre polynomials of zero argument turn into zero for odd values of k. Otherwise $\mathcal{P}(k)$ changes slowly and monotonously.

In view of Eq. (48), it is convenient to rewrite Eqs. (56) and (57) as follows:

$$Y = \chi\,(2\mathcal{E} - \chi) - 1/4, \tag{58}$$

$$Y_\pm = \mathcal{E}(2\chi \pm 1) - \chi^2 + 1/4. \tag{59}$$

In the special case of $\chi = 1/2$ we have

$$\mathcal{P}(k)|_{\chi=1/2} = \frac{(2\mathcal{E}-1)^k (2k)!}{(2\mathcal{E})^{k+1/2}(2^k k!)^2}. \tag{60}$$

The exact formula (55) is not very convenient for big values $k \sim \mathcal{E} \gg 1$, since it contains the Legendre polynomials of high orders. In this case (55) can be replaced by the approximate asymptotical expression [32]

$$f(k) \approx \frac{1}{\sqrt{2\pi k_* r}}\left[\left(\frac{r+Y}{Y_+}\right)^{k_*} + (-1)^k \left(\frac{|Y_-|}{r+Y}\right)^{k_*}\right], \tag{61}$$

where $r = \sqrt{\mathcal{E}^2 - Y - 1/4}$ and $k_* = k + 1/2$. In fact, numerical tests show that approximation (61) is very good even for $k \sim 1$ (provided $\mathcal{E} \gg 1$). It is useful to rewrite Eq. (61) in terms of $\mathcal{E}$ and χ:

$$f(k) \approx \frac{1}{\sqrt{2\pi k_*(\mathcal{E}-\chi)}}\left[\left(\frac{\mathcal{E}(2\chi+1) - (\chi+1/2)^2}{\mathcal{E}(2\chi+1) - \chi^2 + 1/4}\right)^{k_*} + (-1)^k \left(\frac{|\mathcal{E}(2\chi-1) - \chi^2 + 1/4|}{\mathcal{E}(2\chi+1) - (\chi+1/2)^2}\right)^{k_*}\right]. \tag{62}$$

We can simplify the first term inside the square brackets, using the approximation $(1-\varepsilon)^{k_*} \approx \exp(-k_*\varepsilon)$, since the corresponding fraction is very close to unity for $\mathcal{E} \gg 1$. On the other hand, we can replace the second fraction by its limit value for $\mathcal{E} \to \infty$ (assuming that $\chi \ll \mathcal{E}$). Thus we arrive at

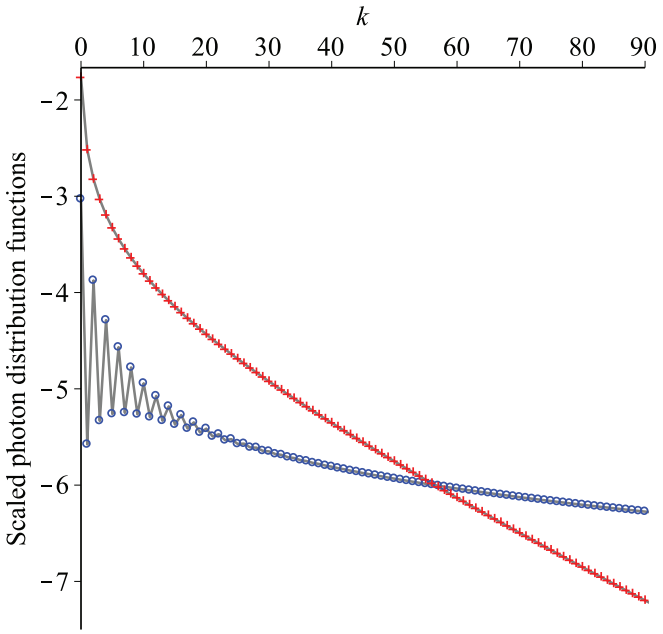

FIG. 7. (Color online) The scaled photon distribution functions $\ln[f_m(k)]$ in the monotone regime of photon generation for the cavity (blue circles ○) and detector (red crosses +). The parameters are: $\beta = g/\omega_0, \nu = \vartheta_2 - 1/2, \gamma = 3\beta\omega_0, \vartheta_1 = \vartheta_2 = 1/2, \beta\omega_0 t = 2$. The mean energies of the modes at this instant are equal to $\mathcal{E}_1 \simeq 394.6$ and $\mathcal{E}_2 \simeq 17.6$.

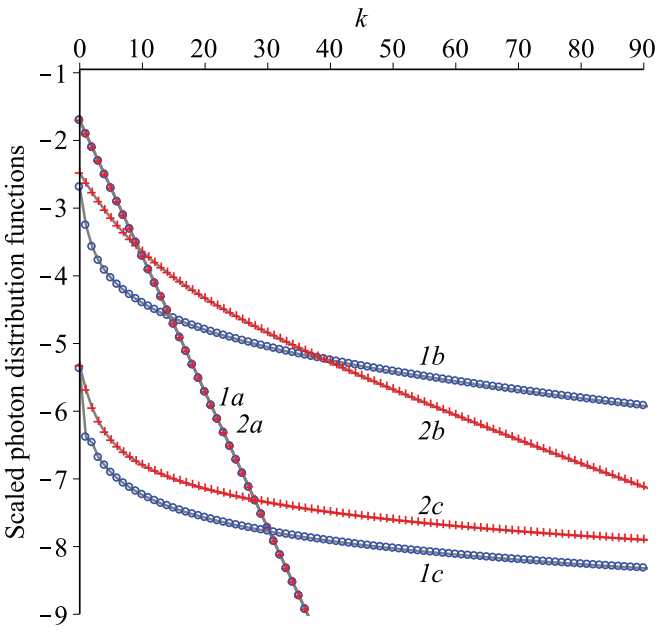

FIG. 8. (Color online) The scaled photon distribution functions $\ln[f_m(k)]$ in the monotone regime of photon generation, at the instants $t_0 = 0$ (a), $t_1 = 1/(\beta\omega_0)$ (b), and $t_3 = 3/(\beta\omega_0)$ (c), for the cavity (blue circles ○) and detector (red crosses +). The parameters are: $g = \beta\omega_0, \nu = \vartheta_2 - 1/2, \gamma = 0.1\beta\omega_0, \vartheta_1 = \vartheta_2 = 5$. Dimensionless mean energies of the cavity mode at different instants of time are as follows: $\mathcal{E}_1(t_0) = 5.00$, $\mathcal{E}_1(t_1) \simeq 93.5$, and $\mathcal{E}_1(t_3) \simeq 29557.4$. For the detector we have $\mathcal{E}_2(t_0) = 5.00$, $\mathcal{E}_2(t_1) \simeq 19.3$, and $\mathcal{E}_2(t_3) \simeq 12765.4$.

the approximate expression

$$f(k) \approx \frac{1}{\sqrt{2\pi k_* \mathcal{E}}}\left[\exp\left(-\frac{k_*}{2\mathcal{E}}\right) + (-1)^k \left|\frac{2\chi - 1}{2\chi + 1}\right|^{k_*}\right]. \quad (63)$$

We see that the squeezing coefficient is responsible for oscillations of the PDF, whereas the mean energy determines the slowly varying part of the PDF, averaged over two adjacent values $f(k)$ and $f(k+1)$. The terms containing the factor $(-1)^k$ in (63) practically do not contribute to the sum $\sum_{k=0}^{\infty} k\mathcal{P}(k)$. Replacing this sum by the integral over dk_* from 0 to ∞ (i.e., using the Euler-MacLaurin approximation), one can easily verify that distribution (63) has correct normalization.

Figure 7 shows PDFs for the field and detector modes in the case of initial vacuum states ($\vartheta_1 = \vartheta_2 = 1/2$), when $\beta\omega_0 t = 2$. We see that the photon distribution of field mode shows clear oscillations. However, no oscillations appear in the detector photon distribution function. Examples of PDFs for initial identical thermal states of the field and detector modes are given in Fig. 8.

VII. FLUCTUATIONS OF PHOTON NUMBERS

One of the quantities characterizing quantum fluctuations is the variance of the number of quanta,

$$\sigma_{\mathfrak{n}} = \sum_{k=1}^{\infty} k^2 \mathcal{P}(k) - \left(\sum_{k=1}^{\infty} k\mathcal{P}(k)\right)^2.$$

For the most general Gaussian states, this variance was calculated in Ref. [31]. In the case under study, the first-order mean values of the quadrature components are equal to zero, and equations of Ref. [31] can be simplified as

$$\sigma_{\mathfrak{n}} = 2(\mathcal{E}^2 - 1/4) - Y, \quad (64)$$

where Y is given by Eqs. (56) or (58). The photon statistics is characterized frequently by the Mandel parameter $Q = (\sigma_{\mathfrak{n}} - \bar{\mathfrak{n}})/\bar{\mathfrak{n}}$, where $\bar{\mathfrak{n}} = \mathcal{E} - 1/2$. However, this parameter is not very useful for the Gaussian states with zero mean values of quadrature components, since it is always greater than unity and (roughly) proportional to $\bar{\mathfrak{n}}$. For the Gaussian states, it is much more interesting to know whether these states are close to thermal states with equal variances of quadrature components and the monotone Planck distribution of photon numbers in the selected mode, or to highly squeezed states with strongly oscillating photon distribution function. It can be shown [12] that the variances of the photon number in the Gaussian states with zero first-order mean values of the quadrature components obey the inequality $\sigma_{\mathfrak{n}} \geqslant \bar{\mathfrak{n}}(\bar{\mathfrak{n}} + 1)$, the equality sign being attained for *thermal* quantum states. On the other hand, for pure squeezed vacuum states we have the equality $\sigma_{\mathfrak{n}}^{(sqzvac)} = 2\bar{\mathfrak{n}}(\bar{\mathfrak{n}} + 1)$. Therefore, the parameter $Z \equiv \sigma_{\mathfrak{n}}/[\bar{\mathfrak{n}}(1 + \bar{\mathfrak{n}})]$ seems to be useful for Gaussian states with zero mean values of quadrature components. If Z is close to unity, the state is close to a thermal one, but if $Z \approx 2$, the state can show strong squeezing. One can see that $\bar{\mathfrak{n}}(1 + \bar{\mathfrak{n}}) = \mathcal{E}^2 - 1/4$. The equivalent expressions

$$Z = 1 + \frac{\mathcal{B}^2}{\mathcal{E}^2 - 1/4} = 2 - \frac{Y}{\mathcal{E}^2 - 1/4} \quad (65)$$

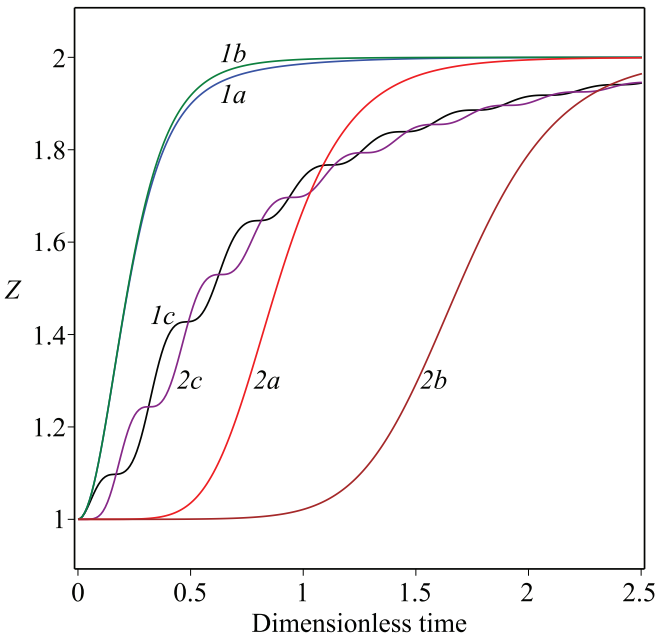

FIG. 9. (Color online) Dimensionless coefficients $Z_{1,2}$ versus the dimensionless time variable $\beta\omega_0 t$ for the cavity (*1*) and detector (*2*) modes in the monotone and oscillating regimes with $\tilde{\nu} = \vartheta_2$ and $\vartheta_1 = \vartheta_2 = 5$. Lines *a* and *b* correspond to $\gamma = 0.1\beta\omega_0$ and $\gamma = 10\beta\omega_0$, respectively, with $\gamma = \beta\omega_0$. Lines *1c* and *2c* correspond to $g = 10\beta\omega_0$ and $\gamma = \beta\omega_0$ (oscillating regime of photon generation).

show that, indeed, Z can vary between the values 1 and 2. Due to Eq. (58), $Z \approx 2 - 2\chi/\mathcal{E}$ if $\mathcal{E} \gg \chi$ and $\mathcal{E} \gg 1$.

The evolution of functions $Z_1(t)$ and $Z_2(t)$ in different regimes is illustrated in Fig. 9.

VIII. DISCUSSION

We have demonstrated that coupling the resonance field mode with a damped oscillator detector can change significantly the photon generation rate and statistical properties of the quantum state of the mode, evolving under the conditions of the dynamical Casimir effect. Moreover, under realistic conditions, statistical properties of the detector quantum state can be quite different from that of the field mode. If the cavity-detector coupling is not too strong, the response of the detector can be observed with a significant delay, compared with the response of the field mode itself. This response diminishes with increase of the damping coefficient in the detector mode. It is curious, nonetheless, that under certain conditions, a stronger damping in the detector can result in a bigger number of photons in the cavity than in the undamped case (provided the intermode coupling is strong enough). These peculiarities can be important for the correct interpretation of experimental results.

In this connection, it is worth discussing the validity of approximations made in the paper, as well as possible realistic values of parameters characterizing the model. Remember that dimensionless damping and coupling coefficients, γ and g, are normalized by the fundamental eigenfrequency ω_0 of the microwave cavity. Therefore $\gamma = (2Q_d)^{-1}$, where Q_d is the quality factor of the detector mode. So we may think that realistic values could be $\gamma \sim 10^{-2}$–10^{-3}. The interval of variations of the coupling coefficient can be estimated as the interval of variations of the cavity eigenfrequency, when the position of antenna (induction loop) is varied inside the cavity. This interval does not exceed usually a few dozens of MHz, so that for the resonance frequency $\omega_0/(2\pi) \sim 2\,\mathrm{GHz}$ we may believe that $g_{\max} \sim 10^{-2}$. For such small values of the dimensionless coupling coefficient, the rotating wave approximation used in the initial Hamiltonian (3) seems to be quite reasonable [34,35]. (For recent studies concerning the conditions of validity of RWA see, e.g., Refs. [36–38].) Note that although the coupling constant and damping coefficient in Figs. 1, 3, and 6 assume formally the values much bigger than unity, they are, in fact, much smaller than ω_0, since in these figures they are normalized by the small frequency modulation depth β, which is expected to be of the order of 10^{-3} or less.

ACKNOWLEDGMENT

The authors acknowledge the partial support of the Brazilian agency CNPq.

[1] V. V. Dodonov, Phys. Scr. **82**, 038105 (2010).
[2] D. A. R. Dalvit, P. A. Maia Neto, and F. D. Mazzitelli, in *Casimir Physics*, edited by D. Dalvit, P. Milonni, D. Roberts, and F. da Rosa, Lecture Notes in Physics Vol. 834 (Springer, Berlin, 2011), p. 419.
[3] P. D. Nation, J. R. Johansson, M. P. Blencowe, and F. Nori, Rev. Mod. Phys. **84**, 1 (2012).
[4] V. V. Dodonov, Phys. Lett. A **207**, 126 (1995).
[5] N. B. Narozhny, A. M. Fedotov, and Yu. E. Lozovik, Phys. Rev. A **64**, 053807 (2001).
[6] W.-J. Kim, J. H. Brownell, and R. Onofrio, Phys. Rev. Lett. **96**, 200402 (2006).
[7] T. Kawakubo and K. Yamamoto, Phys. Rev. A **83**, 013819 (2011).
[8] A. V. Dodonov and V. V. Dodonov, Phys. Rev. A **86**, 015801 (2012).
[9] C. Braggio, G. Bressi, G. Carugno, C. Del Noce, G. Galeazzi, A. Lombardi, A. Palmieri, G. Ruoso, and D. Zanello, Europhys. Lett. **70**, 754 (2005).
[10] C. Braggio, G. Bressi, G. Carugno, F. Della Valle, G. Galeazzi, and G. Ruoso, Nucl. Instr. Meth. A **603**, 451 (2009).
[11] C. Braggio, G. Carugno, F. Della Valle, G. Galeazzi, A. Lombardi, G. Ruoso, and D. Zanello, New J. Phys. **15**, 013044 (2013).

[12] A. S. M. de Castro, A. Cacheffo, and V. V. Dodonov, Phys. Rev. A **87**, 033809 (2013).
[13] A. V. Dodonov and V. V. Dodonov, Phys. Scr. **T153**, 014017 (2013).
[14] A. S. M. de Castro and V. V. Dodonov, J. Phys. A **46**, 395304 (2013).
[15] Y. N. Srivastava, A. Widom, S. Sivasubramanian, and M. P. Ganesh, Phys. Rev. A **74**, 032101 (2006).
[16] J. T. Mendonça, G. Brodin, and M. Marklund, Phys. Lett. A **375**, 2665 (2011).
[17] G. Galeazzi, A. Lombardi, G. Ruoso, C. Braggio, G. Carugno, F. Della Valle, D. Zanello, and V. V. Dodonov, Phys. Rev. A **88**, 053806 (2013).
[18] A. S. M. de Castro, V. V. Dodonov, and S. S. Mizrahi, J. Opt. B: Quantum Semiclass. Opt. **4**, S191 (2002).
[19] E. A. Sete and H. Eleuch, Phys. Rev. A **82**, 043810 (2010).
[20] X. Zhang, T.-Y. Zheng, T. Tian, and S.-M. Pan, Chin. Phys. Lett. **28**, 064202 (2011).
[21] X. Zhang, H. Yang, T. Y. Zheng, and S. M. Pan, Int. J. Theor. Phys. **53**, 510 (2014).
[22] C. K. Law, Phys. Rev. A **49**, 433 (1994).
[23] F. X. Dezael and A. Lambrecht, Europhys. Lett. **89**, 14001 (2010).
[24] D. Faccio and I. Carusotto, Europhys. Lett. **96**, 24006 (2011).
[25] A. V. Dodonov and V. V. Dodonov, Phys. Lett. A **289**, 291 (2001).
[26] A. V. Dodonov, V. V. Dodonov, and S. S. Mizrahi, J. Phys. A **38**, 683 (2005).
[27] V. V. Dodonov, J. Opt. B: Quantum Semiclass. Opt. **4**, R1 (2002).
[28] A. Lukš, V. Peřinová, and Z. Hradil, Acta Phys. Polon. A **74**, 713 (1988).
[29] S. Chaturvedi and V. Srinivasan, Phys. Rev. A **40**, 6095 (1989).
[30] P. Marian, Phys. Rev. A **45**, 2044 (1992).
[31] V. V. Dodonov, O. V. Man'ko, and V. I. Man'ko, Phys. Rev. A **49**, 2993 (1994).
[32] V. V. Dodonov, Phys. Scr. **T140**, 014020 (2010).
[33] V. V. Dodonov and V. I. Man'ko, in *Invariants and the Evolution of Nonstationary Quantum Systems*, edited by M. A. Markov, Proceedings of Lebedev Physics Institute (Nova Science, Commack, New York, 1989), Vol. 183.
[34] M. O. Scully and M. S. Zubairy, *Quantum Optics* (Cambridge University Press, Cambridge, 1997).
[35] W. Vogel and D.-G. Welsch, *Quantum Optics* (Wiley-VCH, Weinheim, 2006).
[36] A. B. Klimov, I. Sainz, and S. M. Chumakov, Phys. Rev. A **68**, 063811 (2003).
[37] T. Werlang, A. V. Dodonov, E. I. Duzzioni, and C. J. Villas-Bôas, Phys. Rev. A **78**, 053805 (2008).
[38] C. Fleming, N. I. Cummings, C. Anastopoulos, and B. L. Hu, J. Phys. A **43**, 405304 (2010).